

WEAR- AND CORROSION-RESISTANT STEELS CONTAINING NIOBIUM CARBIDE

M. Seifert¹, S. Huth^{1,2}, S. Siebert¹ and W. Theisen¹

¹Ruhr-Universität Bochum, Chair of Materials Technology,
Universitätsstr. 150, Bochum, 44801, Germany
²now at Hilti AG, Corporate Research & Technology,
Feldkircherstr. 100, Schaan, 9494, Liechtenstein

Keywords: Niobium Carbide, Martensitic Stainless Steels, Bearing Steels, PM Steels, Steels for Polymer Industry, Thermodynamic Equilibrium Calculations, Diffusion Alloying, Manufacturing

Abstract

Niobium, like titanium and vanadium, forms super-hard mono-carbides (MC) which remain relatively pure in Fe-base alloys on account of their low solubility for other metallic alloying elements. Because the super-hard mono-carbides have a higher hardness than the precipitated chromium carbides commonly used in wear-resistant alloys, they are suitable as alternative hard phases.

This paper deals with new wear- and corrosion-resistant steels containing niobium carbide that were produced by ingot and powder metallurgy (PM) for use as plastic mould and bearing steels. Based on equilibrium calculations by CALPHAD (CALculation of PHase Diagrams) methods, the microstructures developed during the production of these steels were analysed, and the results are discussed with respect to important properties such as abrasive wear and corrosion resistance. Alloys can be produced by precipitation of primary niobium carbides of the MC type, which are embedded in a martensitic metal matrix that can be subjected to secondary hardening. Because of the high affinity of niobium for carbon, the formation of chromium carbides can be suppressed even in high-chromium alloys, thus leaving chromium contents of more than 12 wt.% in the metal matrix as are required to impart corrosion resistance. This allows the production of stainless, wear-resistant cold-work tool steels for the food processing and pharmaceutical industries, as well as corrosion-resistant bearing steels.

Introduction

It is commonly known that martensitically hardenable Fe-Cr-C alloys with a considerable amount of carbides show good resistance to abrasive wear [1,2]. One group among these alloys is tool steels with a carbon content up to 2 wt.%. Above a critical carbon content, eutectic carbides form during solidification. These can be iron-rich M_3C , or chromium-rich M_7C_3 if the chromium content is high enough. The eutectic network tends to be coarse. Additionally, the carbide morphology is unfavourable and the amount increases with increasing carbon content. A high amount of coarse carbides is positive for the wear resistance, but impairs the ductility and the fracture toughness. This becomes worse if the eutectic content is so high that it forms a network that surrounds the more ductile metal cells, which leads to pre-defined crack paths [3]. In general, hard phases are able to reduce abrasive wear, if they are harder than the abrading particles. Thus, for many

applications, the carbides mentioned above are too soft and harder carbides would be preferred [4].

This can be improved by alloying steels with certain amounts of vanadium, niobium or titanium. These form MC type carbides with a hardness >2200 HV that precipitate primarily from the melt, even for alloying comparatively small amounts of these refractory metals [2,5]. Depending on the alloying content, this may lead to very large carbides [2]. Among these elements, niobium is the most promising element for several applications: it has almost no solubility in the iron matrix and thus does not contribute to secondary hardening [6,7]. This means that the amount of NbC and carbon needed for precipitation can be adjusted quite precisely. Furthermore, NbC precipitates have a lower solubility for the main alloying elements such as chromium and molybdenum than comparable carbides like TiC and VC. This means that higher amounts of those alloying elements remain dissolved in the matrix. This is especially interesting for corrosion-resistant steels that also require a considerable wear resistance, eg extruders in the polymer industry or cutting tools in the food industry [8 and references therein], because there is no chromium depletion around NbC.

The alloying strategy for martensitic stainless steels with good wear resistance is complex because these properties are somewhat contradictory. As in hardenable tool steels, hardness and wear resistance require a certain amount of carbon, and the corrosion resistance is in need of at least 10.5 wt.%Cr dissolved in the matrix [9]. As mentioned above, chromium is usually also required to precipitate carbides and so the alloying content of chromium has to be increased. This is only possible up to a certain amount because chromium stabilises ferrite and thus hinders martensitic transformation at very high amounts. Even though these three key properties can be adjusted within a wide range by an adequate heat treatment, there is only a limited possibility to keep all of them at a high level. As already mentioned, niobium can help to retain more chromium in the matrix and depress the well-known depletion around chromium-rich carbides [10,11].

The size of primary NbC precipitates is disadvantageous, not only for forging, but probably also for the corrosion resistance in some applications, eg for pitting corrosion. Adequate manufacturing routes for steels containing a high amount of NbC thus have to be developed. In this study, we focus on a new powder metallurgical manufacturing route that leads to two different concepts for corrosion- and wear-resistant steels. One of these is aimed at applications in the polymer industry, the other is being developed for bearings in sea water environments.

Martensitic Stainless PM Steels with Enhanced Wear and Corrosion Resistance

Development

The basic alloy system of this corrosion-resistant cold-work tool steel is Fe-Cr-Nb-Mo-C. As already mentioned, a chromium content of at least 10.5 wt.% is sufficient to ensure corrosion resistance [9] because chromium then transfers its passivation ability to the iron matrix [12]. This leads to the formation of a Cr₂O₃ layer that isolates the metal from the surrounding medium. If the corrosion resistance has to be high, the proportion of carbon and chromium has to be adjusted so that chromium-rich carbides are avoided. These withdraw chromium from the matrix, thus the Cr content in it is reduced. Furthermore, a zone with a strong chromium depletion surrounds the carbides [10,11], which is especially detrimental for resistance against pitting corrosion.

The niobium content can be more or less arbitrarily adjusted to the intended content of NbC. In corrosion-resistant steels, the carbon content has to be balanced to: (i) form the intended amount of NbC, (ii) avoid chromium-rich carbides and (iii) achieve a hardenable matrix, ie a sufficient amount of carbon has to be dissolved in the matrix at the austenitisation temperature (T_{Aus}). After an adequate heat treatment, this will lead to NbC precipitates embedded in a stainless martensitic matrix [13].

Molybdenum is added to further increase the corrosion resistance, especially against pitting corrosion. There are ongoing discussions on how molybdenum actually increases the corrosion resistance in steels and it seems to be clear that it only shows its positive effects in combination with a sufficient amount of chromium [14–17]. At higher contents, molybdenum tends to segregate, which might lead to the precipitation of molybdenum-rich M_6C [1]. Naturally, these features are unwanted in stainless steels.

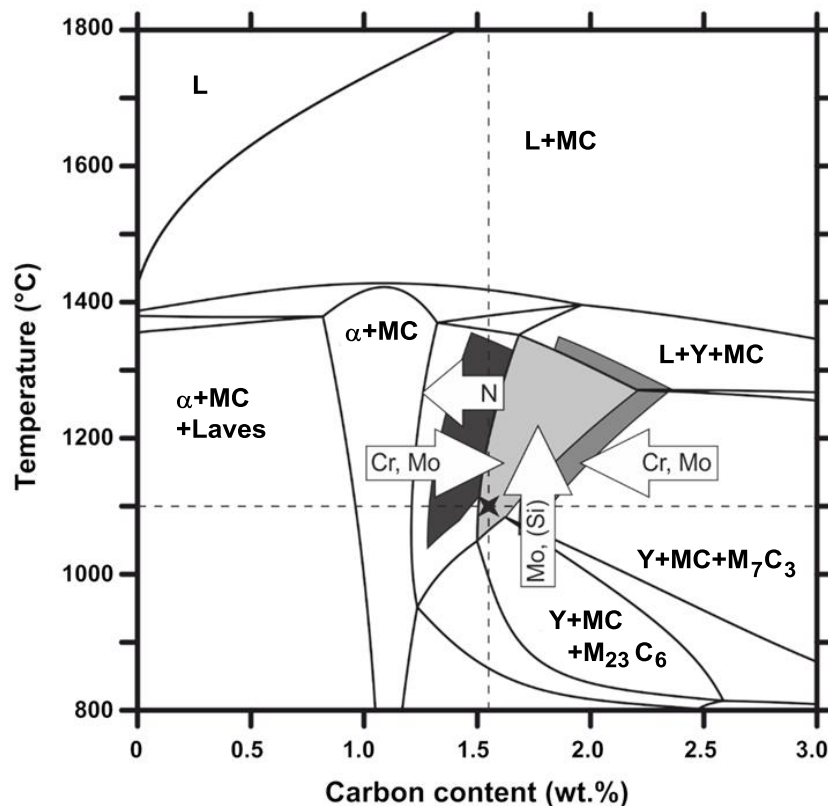


Figure 1. Quasi-binary phase diagram of the Fe-12Cr-10Nb-2Mo system depending on the carbon content (L=liquid, MC=NbC, α =Ferrite, γ =Austenite). The target phase field, γ +MC, is coloured in light grey. The influence of less and more niobium is shown by the shift of this phase field to lower carbon contents (9 wt.%Nb, dark grey) and to higher carbon contents (12 wt.%Nb, medium grey), respectively. The arrows indicate the influence of the addition of chromium, molybdenum, nitrogen and silicon on the target phase field. The dashed lines indicate a possible austenitisation temperature of 1100 °C for a carbon content of 1.55 wt.%.

These considerations led to a steel with 12 wt.%Cr, 10 wt.%Nb and 2 wt.%Mo [18,19]. A phase diagram calculated with the commercial software Thermo-Calc Version S in combination with the

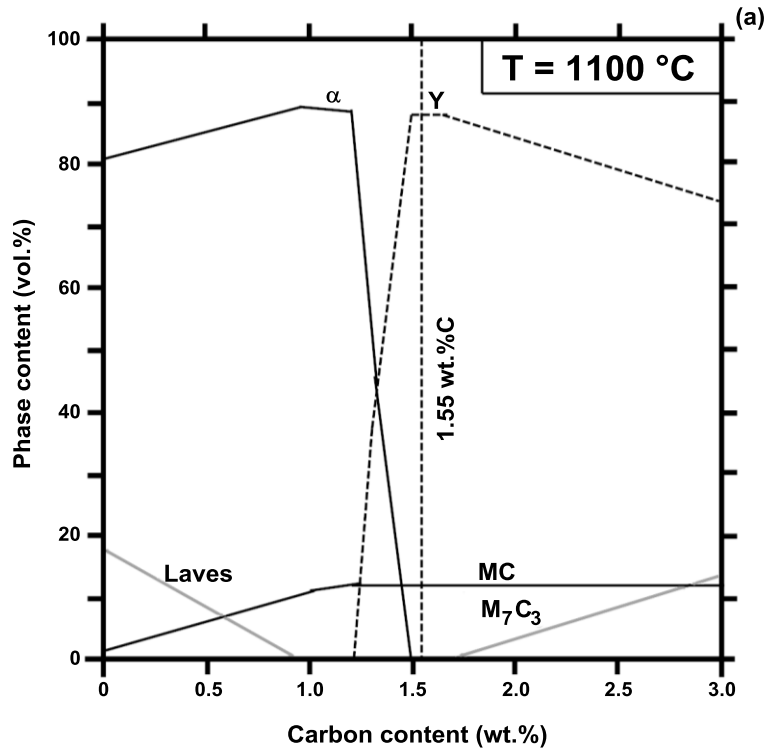
database TCFE7 is shown in Figure 1. The target phase field for a corrosion-resistant martensite containing only NbC is γ +MC coloured in light grey. The influence of different niobium contents is shown by the shift of this phase field, ie lower contents require less carbon (dark grey), higher contents require more carbon (medium grey). Arrows depict the influence of adding other alloying elements. Chromium and molybdenum clearly reduce the size of the γ +MC phase field because they both stabilise the ferrite and also lead to chromium-rich carbides. At higher amounts of molybdenum, ie above ≈ 3 wt.%, precipitation of M_6C becomes possible, which shrinks the target field from the bottom. Nitrogen, introduced either by atomisation with nitrogen gas or intentional alloying, widens the γ +MC field in the direction of lower carbon contents, whereas the right boundary remains constant. Manganese and silicon do not have any distinct influence on this alloy for contents usually introduced in the scrap used for melting the steel [18]. However, an unfavourable combination of too much silicon with certain amounts of chromium and molybdenum will lead to the stabilisation of M_6C , which shrinks the target phase field as already mentioned. It is obvious that a T_{Aus} of at least 1100 °C is necessary to safely hit the γ +MC phase field (see the dashed line). Even at 1100 °C, the possible carbon content is fairly limited at around 1.5–1.7 wt.% (dashed line indicates 1.55 wt.% in Figure 1). Lower austenitisation temperatures, as well as excessive carbon contents, would lead to the precipitation of chromium-rich carbides. However, this would probably be beneficial for applications demanding enhanced wear resistance [18]. A much higher T_{Aus} would lead to more retained austenite (RA) due to the higher difference in temperature and to coarsening of the microstructure [1]. The general hardenability of steels can be estimated by calculating the martensite-start temperature (M_s) and taking account of the composition of the matrix at T_{Aus} . This can be achieved using Equation 1, which was developed by Andrews [20] and subsequently modified by Kung and Rayment [21] and Berns and Krasokha [22] (composition in wt.%):

$$M_s = 539 - 423 \cdot (C+N) - 30.4 \cdot Mn - 17.7 \cdot Ni - 12.1 \cdot Cr - 7.5 \cdot Mo - (-7.5 \cdot Si + 10 \cdot Co) \quad (1)$$

Figure 2 shows three equilibrium calculations at a possible T_{Aus} of 1100 °C and displays valuable information for the design of this steel. Figure 2(a) visualises the content of the stable phase depending on the carbon content. Besides the information gathered from Figure 1, the content of MC within the γ +MC-field can be estimated to be about 12 vol.%, which remains constant for higher carbon contents. Furthermore, the amount of MC, and with it the carbon content, stays almost constant with rising temperature (not shown here) owing to the low solubility of NbC in the matrix [23]. Figure 2(b) shows the atomic composition of the MC with increasing carbon content. According to the employed database, it can clearly be seen that the MC phase is almost purely Nb(C,N) for a carbon content of 1.55 wt.%. Only very small amounts of chromium, molybdenum and iron are dissolved in the MC. However, their amount slightly increases with increasing carbon content. Figure 2(c) shows the composition of the matrix with increasing carbon content. The x axis is scaled only from 1.0 to 3.0 wt.%C because the austenite is not stable below ≈ 1.2 wt.%, as shown in the diagram. For a carbon content of 1.55 wt%, the matrix contains about 0.35 wt.%C, which is sufficient for a high hardness [1]. Additionally, the highest amounts of chromium (≈ 13.2 wt.%) and molybdenum (≈ 2.4 wt.%) are dissolved in the matrix at the intended carbon content of 1.55 wt.%. This leads to a pitting resistance equivalent number (PREN) of 21.4. The PREN is commonly used to estimate the resistance of a steel against pitting corrosion or to at least to compare different steels. It is calculated using Equation 2 (in wt.%) [24,25]. The matrix contains almost no niobium or nitrogen.

$$\text{PREN} = \text{Cr} + 3.3 \cdot \text{Mo} + 20 \cdot \text{N} \quad (2)$$

Although Figure 2 indicates that no nitrogen is dissolved in the matrix, about 0.12 wt.% was detected experimentally [18]. This seems to be an inconsistency in the database used for the calculation. However, presumably the PREN is the only property that would differ slightly due to this. The nitrogen content in the Nb(C,N) is replaced by carbon, leading to a decreased carbon content in the matrix [26]. Nitrogen dissolved in the matrix has a positive influence on the PREN. Additionally, it contributes to the hardenability of the steel [27].



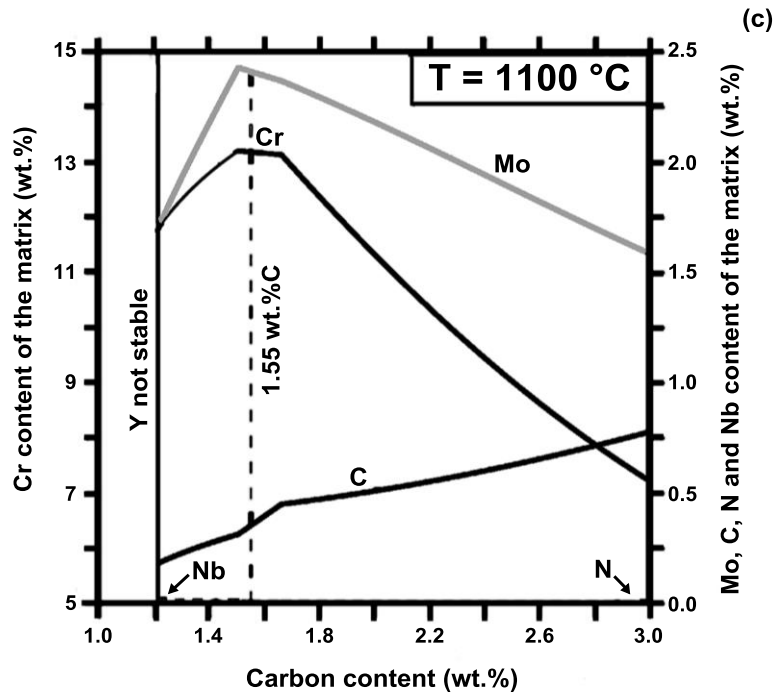
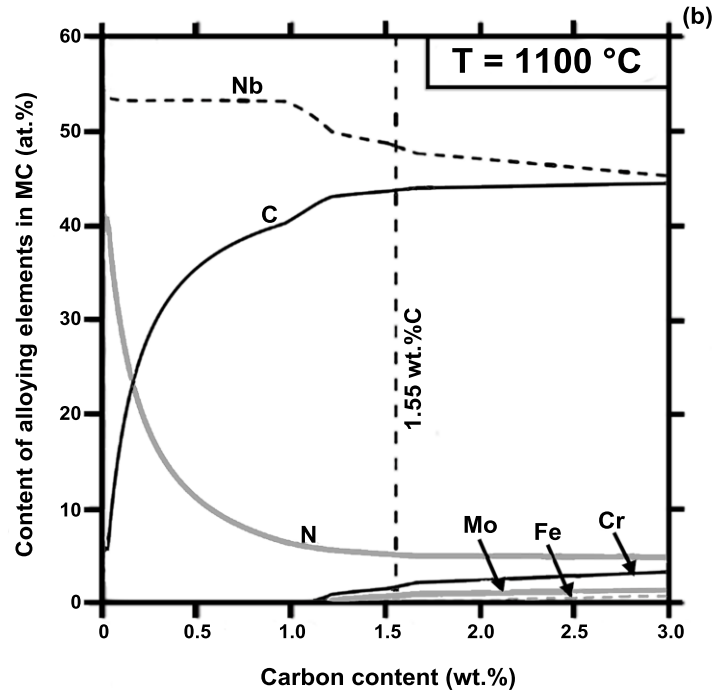


Figure 2. Different equilibrium properties at 1100 °C depending on the carbon content calculated with Thermo-Calc. The dashed line indicates a carbon content of interest for this study; (a) Phase content in vol.%, (b) Composition of the NbC, (c) Composition of the matrix. The x axis in (c) is scaled only from 1.0 to 3.0 wt.%C because the austenite is not stable below ≈ 1.2 wt.%, which is also shown in the diagram.

Figure 1 shows that the liquidus temperature of the NbC for the intended carbon content is higher than 1800 °C in this system. This means that these would precipitate directly from the melt at a very early stage of solidification. Huge carbides comparable to those in Figure 3(a) would be the consequence of this [2]. However, for rapid solidification, eg in welding seams, a fine dispersion of NbC is achievable, as can be seen in Figure 3(b) for a hardfacing alloy, which also clearly shows the martensitic structure of the matrix. A possible way to obtain a comparable microstructure is provided by powder metallurgy. However, in a melt conventionally designed for atomisation, the NbC would grow as large as mentioned above and would thus clog the nozzle and the atomisation would stop [28]. A possible way to overcome this is a process route called diffusion alloying [18,29,30].

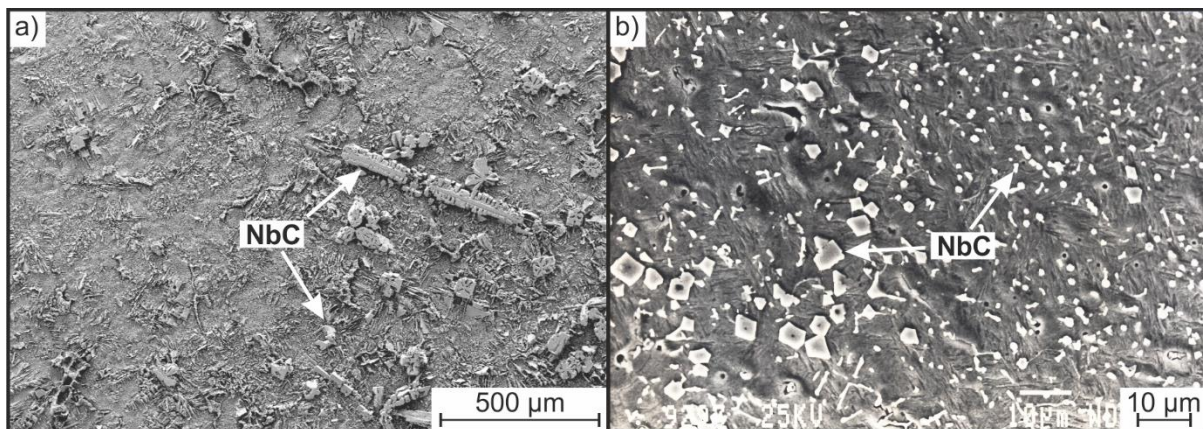


Figure 3. Different morphologies of NbC; (a) huge NbC in alloy G-X130NbCrMoW6-4-2-2 in the as-cast condition, (b) fine dispersion of NbC, comparable to a powder metallurgical microstructure, in hardfacing alloy X120NbCrMoV6-5-2-1.

Diffusion Alloying

Diffusion alloying is based on the idea of atomising a melt that is free of carbon. The resulting carbon-free powder can be mixed with a variable amount of interstitial elements, ie carbon, nitrogen or boron, from a gaseous or solid donor [30]. Consequently, different alloying concepts can be obtained with one base powder, leading to a higher corrosion resistance or wear resistance. The steels under investigation in this study were mixed with graphite, which ideally completely covers the surface of all powder particles after mixing.

The actual process of alloying the carbon-free powder with carbon takes place subsequently during hot isostatic pressing (HIP). At a high pressure of about 100 MPa and typical temperatures of about 1150 °C, the graphite presumably reacts with the oxygen contained in the surface oxides of the steel to form CO and/or CO₂ [18]. This gas phase distributes the carbon uniformly throughout the steel via the pores that initially represent an open porosity. Thus, the process of alloying actually takes place via the gas phase. Due to the high temperature, the carbonization step finishes after a few minutes. Although this cannot really be proven yet, other studies appear to support this theory [32]. The process route of diffusion alloying, including the HIP process, is shown schematically in Figure 4.

To improve the resistance to coarse abrasive wear, additional large NbC particles can be mixed into the powder of the existing alloying concept [13]. Such additions significantly change neither the composition of the matrix nor that of the NbC during diffusion alloying. Depending on the application, the content of admixed NbC can be varied like the content of carbon without losing the intended corrosion resistance.

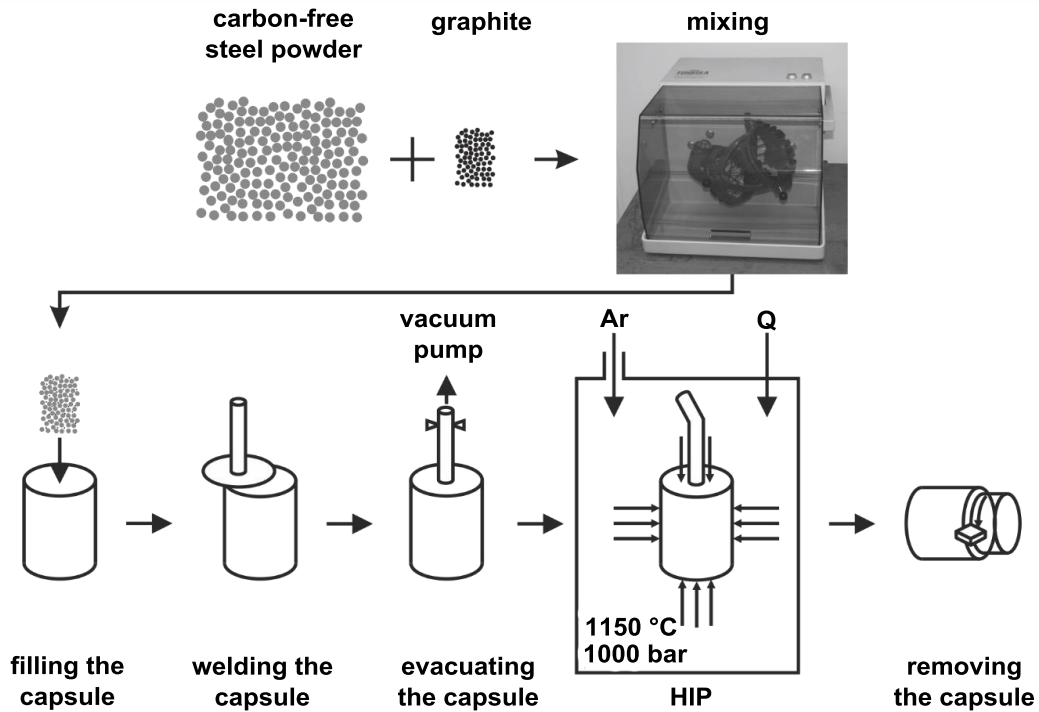


Figure 4. Schematic sequence of diffusion alloying including the HIP process, where Q indicates heat (according to [31]).

Experimental

Heat Treatment. Tempering curves were determined with specimens that were prepared after HIP, austenitised at 1100 °C for 30 minutes and quenched in oil. As indicated in Figure 1, this should lead to a microstructure free of chromium-rich carbides. In conjunction with the information shown in Figure 2, it can be concluded that virtually all the chromium and molybdenum are dissolved in the matrix. Subsequent tempering was conducted sequentially at 150, 200, 300, 400, 450, 500, 520, 540, 560, 580 and 600 °C for two hours each. The Vickers hardness was measured with a load of 294.1 N (HV 30). At least five indents per specimen were measured to enable the calculation of a mean value and a standard deviation.

Wear Tests. The wear resistance was measured using pin-on-grinding paper tests. The specimens were quenched and tempered at the secondary hardness maximum (SHM) to obtain their maximum wear resistance. They were used in the testing rig as a slowly rotating cylinder that was moved along a meandering path across a grinding paper without any overlaps. A schematic illustration of this test is shown in Figure 5, including the area of the specimen (A), the normal force F_N applied

to the specimen, its rotational speed ω and the feed rate v of the grinding paper, ie the table. Flint (SiO_2) with a mesh size of 220 and 80 as well as corundum (Al_2O_3) with a mesh-size of 220 were used as abrasive grinding papers. The mass loss Δm , the density ρ and the length of the wear track l were determined for the calculation of the wear resistance, W_R , using Equation 3. Additionally, scratch tests were performed using the same abrasive for a better understanding of the effective wear mechanisms.

$$W_R = \frac{\rho \cdot A \cdot l}{\Delta m} \quad (3)$$

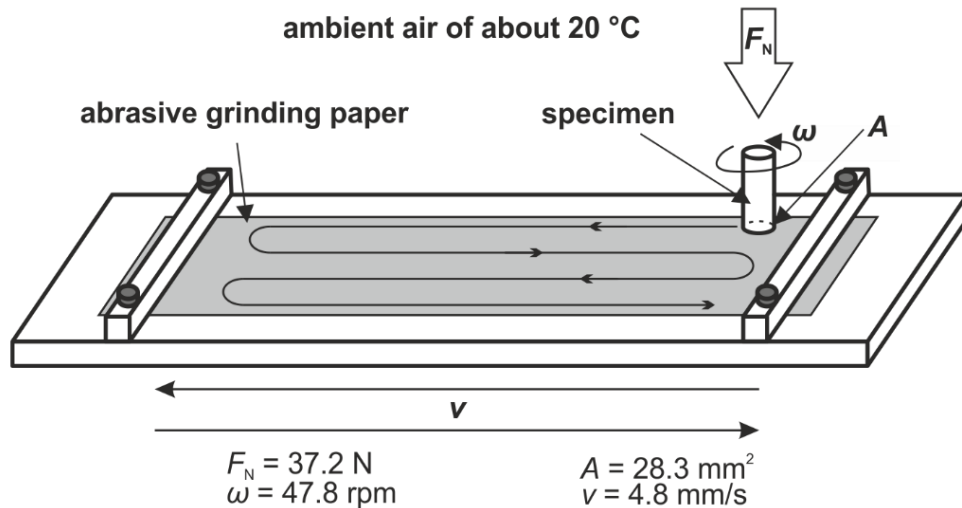


Figure 5. Schematic illustration of the pin-on-grinding paper test. The grinding paper is flint (SiO_2) of mesh size 220 and 80 or corundum (Al_2O_3) with a mesh size of 220. The area A of the specimen is given in the caption as well as the normal force F_N applied to the specimen, the rotational speed ω of the specimen and the feed rate v of the grinding paper (table).

Corrosion Tests. The corrosion resistance was tested in the as-quenched condition for $T_{\text{Aus}} = 1100 \text{ }^\circ\text{C}$. After this heat treatment, a wire was spot-welded onto the rear face of the specimens to provide an electrical contact. The specimens were then embedded in a polymer resin and ground on SiC emery paper of mesh size 1000. To avoid crevice corrosion, the gap between the specimen and the resin was covered with a commercially available lacquer. The exposed conductive surface of the specimens was subsequently measured.

These specimens were used as the working electrode in the corrosion cell. The other components of the cell are a counter electrode of platinum and a calomel reference electrode (Hg_2Cl_2 , +244 mV to the standard hydrogen electrode (SHE)). The latter is inserted in a separate glass vessel that is connected to the cell by a salt bridge that ends in a Haber-Luggin capillary directly in front of the surface of the specimen. A porous frit is used in the salt bridge to avoid contamination by the cell electrolyte. All three electrodes are connected to a potentiostat of type PGP 201 or PGZ 301 (from Voltalab, now Radiometer Analytical) that is connected to a PC. A gas outlet tube is also inserted into the cell. The electrolyte was either 0.5 molar (5%) sulphuric acid (H_2SO_4 , uniform surface

corrosion) or 0.6 molar (3%) sodium chloride (NaCl, pitting corrosion), respectively. The test setup is schematically shown in Figure 6, in which the electrolyte is coloured in grey.

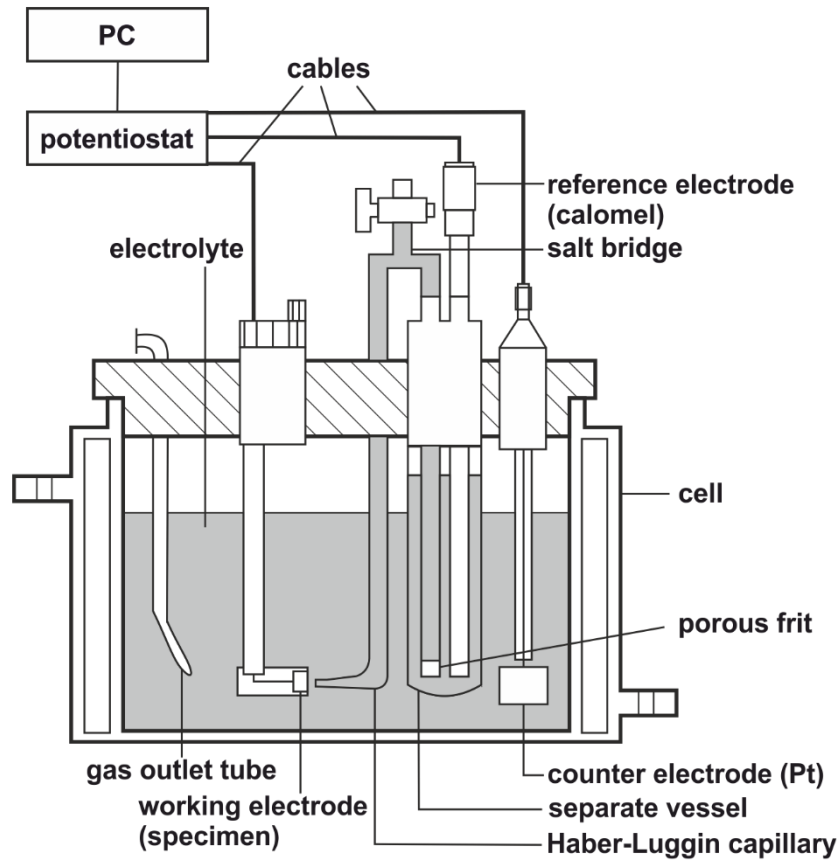


Figure 6. Schematic illustration of the corrosion test setup used to measure potentiodynamic polarisation curves. The electrolyte – either H_2SO_4 or NaCl – is coloured in grey.

Before starting the experiment, the electrolyte was purged with gaseous nitrogen for 30 minutes to remove most of the oxygen. The specimen was then cathodically polarised for 60 seconds at -1 to -1.5 V/SHE to clean the surface and at least to partially eliminate the oxide layer on the surface. This step was followed by the measurement of the open circuit potential (OCP) for 30 minutes. Meanwhile, the oxide layer reformed due to the remaining oxygen in the electrolyte. Subsequently, the potentiodynamic polarisation curve was recorded starting at 10 mV below the OCP with a potential step rate of 600 mV/h. The tests were performed at least twice to confirm reproducibility [33]. The measured potentials are given with respect to SHE. From these curves, different characteristic values were evaluated, such as the passive current density and different passivation potentials for H_2SO_4 and a threshold potential for NaCl indicating pitting corrosion. This latter was evaluated at the potential above which the current density remained higher than $100 \mu\text{A}/\text{cm}^2$ [34,35].

Results and Discussion

Alloy Composition. Preliminary investigations revealed that the calculations based on Thermo-Calc somehow led to incorrect results. Although the target phase field of γ +MC was reached, this was at considerably lower carbon contents than assumed [18]. Thus, the actual corrosion-resistant cold-work tool steel, named PSH1 below, does not contain 1.55 wt.%C, but 1.4 wt.%C. Its composition in wt.% is shown in Table I. All other calculations seem to be valid in the range of this carbon content. The other alloy in this study is a metal matrix composite (MMC) containing PSH1 admixed with 10 vol.%NbC, Table I. This alloy is named MMC in the following. Its carbon content is 1.5 wt.%, which is slightly higher than that of PSH1.

Table I. Composition of the Investigated Alloys (wt.%). Content of admixed NbC (vol.%)

	Fe	Cr	Nb	Mo	C	N	Mn	Si	Vol.% NbC
PSH1	bal.	11.8	10.6	2.3	1.4	0.2	0.4	0.4	-/-
MMC	bal.	11.8	10.6	2.3	1.5	0.2	0.4	0.4	10

Hardness and Microstructure. The microstructures of the as-quenched specimens are shown in Figure 7, which were taken with a scanning electron microscope (SEM) type GEMINI LEO 1530 VP. The fine dispersion of NbC that precipitated during diffusion alloying is obvious in PSH1, Figure 7(a). Their diameter is in the range of 1 – 3 μm , which is even smaller than in the hardfacing alloy shown in Figure 3(b). Figure 7(b) shows the microstructure of the MMC with admixed NbC. Although the precipitated NbC are still finely dispersed here, the distribution of the coarser admixed NbC is not totally homogeneous. Their diameter is about 10 μm , ie they are one order of magnitude larger. This should have a positive effect on the wear resistance of this material.

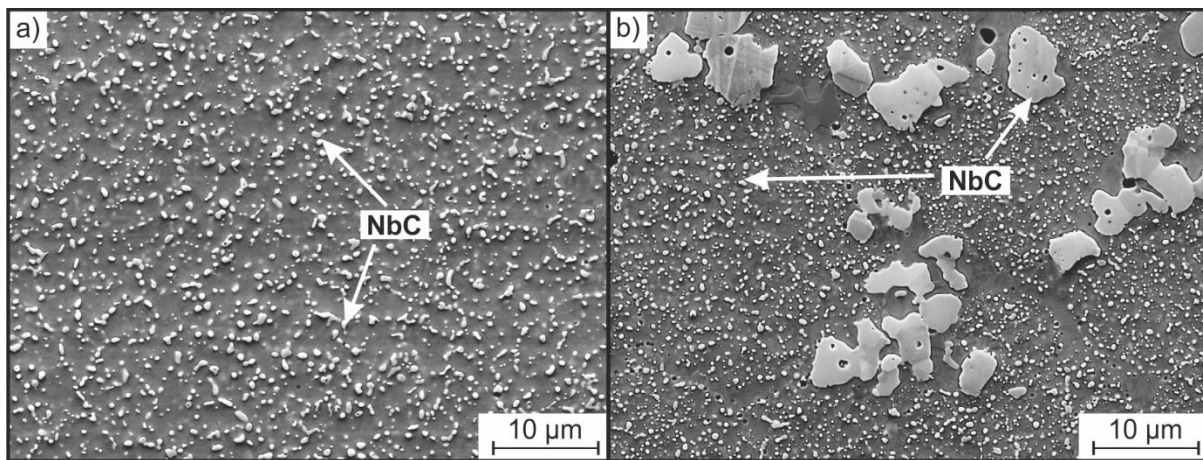


Figure 7. SEM images of the microstructure of; (a) PSH1 and (b) MMC [18] after HIP in the as-quenched condition ($T_{\text{Aus}} = 1100\text{ }^{\circ}\text{C}$). The finely dispersed NbC that precipitated during diffusion alloying have a diameter in the range of 1–3 μm and are thus even smaller than in the hardfacing alloy, Figure 3(b). The admixed NbC in the MMC are considerably larger (about 10 μm in diameter). Their distribution is not totally homogeneous.

Figure 8 shows the tempering curves for both investigated alloys. It is obvious that both reach almost the same hardness after quenching from $T_{\text{Aus}} = 1100\text{ }^{\circ}\text{C}$. This seems reasonable with respect

to their very similar compositions. The slightly higher hardness of the MMC, ie 730 HV 30 in comparison to 710 HV 30, should be the result of the slightly enhanced carbon content in combination with the admixed NbC. Both steels contain small amounts of RA after quenching. According to Equation 1, its content should increase with increasing carbon content. However, the matrix of MMC might also be slightly depleted in chromium, which could compensate for the higher carbon content [13]. The increase in hardness of PSH1 to 750 HV 30 for tempering at 150 °C could be due to the precipitation of small Fe₂C [36–38]. This could overcompensate the loss in hardness due to tempering at low temperatures, by a decrease in the internal stresses [1].

Both steels exhibit a SHM at 520 °C that is associated with the high amount of molybdenum and chromium dissolved in the metallic matrix [13]. In this case, the PSH1 reaches 700 HV 30 and the MMC reaches 770 HV 30. The SHM of the MMC is considerably more pronounced owing to its higher carbon content. This increase in hardness can be explained by the precipitation of M₂C that is rich in chromium and molybdenum [39]. Niobium does not contribute to the SHM due to its low solubility in the steel matrix [6,7].

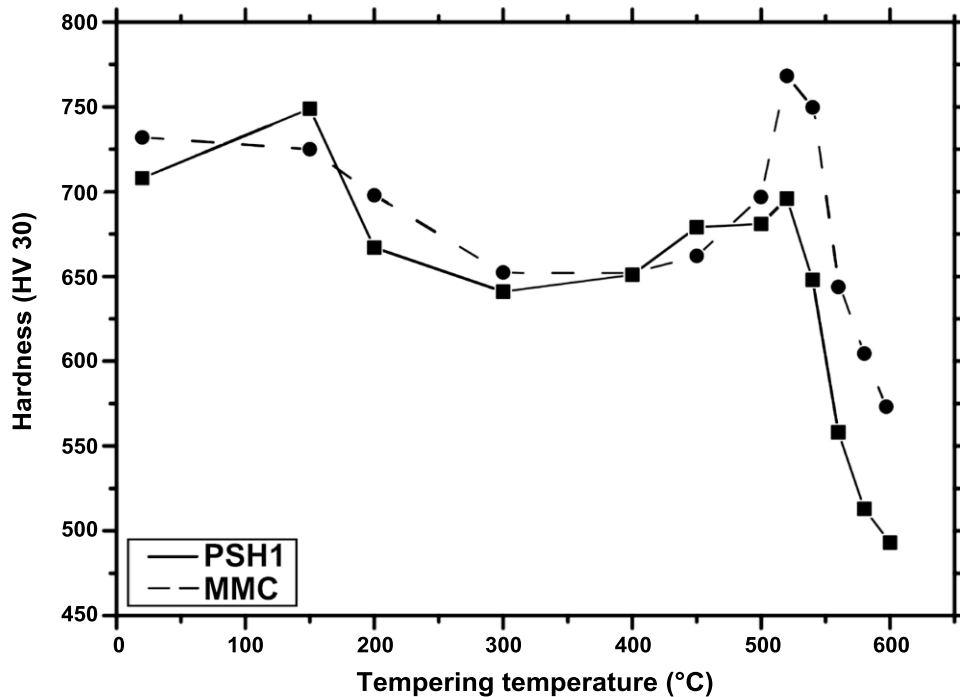


Figure 8. Tempering curves for the two investigated alloys PSH1 and MMC in the range from room temperature to 600 °C for hardening from 1100 °C. The as-quenched hardness of both steels is comparable. The SHM is reached for tempering at 520 °C with MMC and achieves a higher hardness than PSH1.

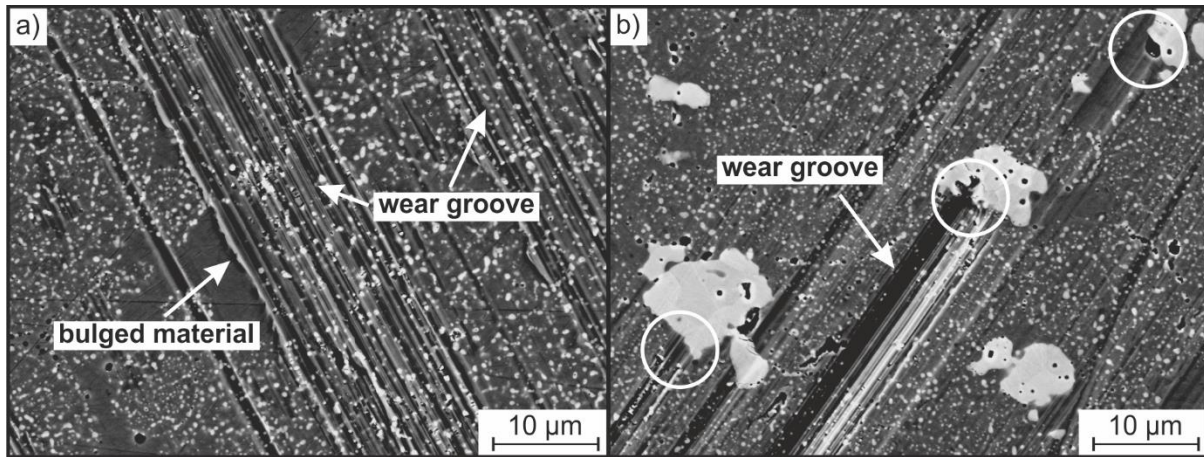


Figure 9. SEM images of worn surfaces of a) PSH1, b) MMC after scratch tests with flint 220. The wear grooves and bulged material at the edge of the grooves are obvious in PSH1. In the MMC, sections of the wear groove indicated by circles show where the abrasive particles were stopped or deflected.

Wear Resistance. Figure 9(a) shows a SEM image of a worn surface of PSH1 after a scratch test against flint 220. The wear groove caused by the abrasive is obvious. In PSH1, the precipitated NbC are the only hard phases in the microstructure. These are much smaller than the abrasive grains and are thus chipped out with the matrix, which is in good agreement with the findings of Axén and Zum Gahr [40]. Whereas the main wear mechanism is micro-cutting, the edges of the groove show very little micro-ploughing, as indicated by bulged material. The precipitated NbC do efficiently support the matrix in a way that the wear grooves are reduced. This view is corroborated by areas that do not contain NbC in which the wear grooves appeared to be deeper and wider, indicating their positive influence due to two-phase hardening of the matrix [13,18]. This can also be explained by a theory proposed by Axén and Zum Gahr, who correlated a decrease in abrasion with a decrease in the free matrix length between carbides [40]. This in turn correlates with a decrease in size and an increase in the number of hard phases [13], both of which are favoured by the manufacturing route performed for the steels in this study, ie diffusion alloying. Some parts of the wear groove indicate that the NbC grooved the abrasive flint particles [13,18]. Because the hardness of flint is considerably lower than that of NbC, this is in good agreement with [40].

The SEM image in Figure 9(b) depicts the effect of admixed niobium carbides on the wear behaviour of the MMC in a scratch test against flint 220. Even though the admixed NbC in this part of the microstructure are somehow smaller than those in Figure 7, they are able to stop or at least deflect the abrasive flint particles, which is indicated by circles in the image. Obviously, this leads to reduced dimensions of the wear grooves in comparison to those in PSH1. This can be correlated with the increased size of the hard phases, which leads to a change in the mechanism of wear protection from matrix hardening to deflecting the wear path [13,18]. Sometimes the large admixed carbides are broken due to micro-cracking. This might be explained by the minor support of the matrix that is actually soft in comparison to the NbC. This can cause plastic deformation at the edges of the large NbC, which leads to cracks due to their low toughness [13]. The addition of NbC to PSH1 thus leads to a far better resistance against coarse abrasive wear, which opens other fields of applications for this alloy [18].

In general, both alloys show the highest wear resistance against flint 220, followed by flint 80 and corundum 220 [13,18]. The considerably larger particles of flint 80 have a negative influence on the wear resistance, especially for the MMC. This is because the effect of larger carbides decreases with increasing abrasive particle size. For PSH1, the wear rate remains almost constant because the size of the abrasive particles in flint 220 is already much larger than that of the precipitated NbC. Thus, no further degradation is observed [13]. The abrasive wear of corundum is lowered but not stopped, as shown for flint 220. Many of the admixed NbC show crack networks and most of them are subject to micro-cutting. Some NbC are even gouged out of the matrix. This is in agreement with [40] because the hardness of corundum and NbC is similar.

One possible application for corrosion-resistant cold-work tool steels such as the PSH1 and the MMC in this study is for processing of polymers [13]. Here, abrasion is the main wear mechanism. Naturally, the actual wear behaviour in a certain application and in an experiment differs for several reasons. Additionally, the pin-on-grinding paper test does not include interdependencies such as corrosion or tribochemical reactions. However, the results of PSH1 and MMC were compared to those obtained with other alloys subjected to the same testing procedure. This is shown in Figure 10 for the alloys 1.4112 (X90CrMoV18, AISI 440B), Böhler M390 (X190CrVMo20-4-1), 1.2379 (X155CrVMo12-1, AISI D2) and Ni-Hard IV (G-X300CrNiSi9-5-2, EN-JN2049) for testing against flint 80. All materials were tested in the quenched and tempered condition, for which they reach their maximum wear resistance. The 1.4112 alloy is a conventionally cast corrosion-resistant cold-work tool steel containing coarse chromium-rich carbides. Böhler M390 is a powder metallurgical corrosion-resistant tool steel containing a high amount of chromium-rich carbides together with 2-3 vol.% VC that are finely dispersed in the martensitic matrix. The 1.2379 alloy is not corrosion-resistant but is only a wear-resistant cold-work tool steel containing coarse chromium-rich, as well as vanadium-rich carbides. Ni-Hard IV is a white cast iron with a high wear resistance due to its high hardness and coarse chromium-rich carbides. It is obvious that the PSH1 almost reaches the level of the common comparable alloy M390 [18,41]. However, the wear resistance of the MMC is superior to all other tested alloys [2].

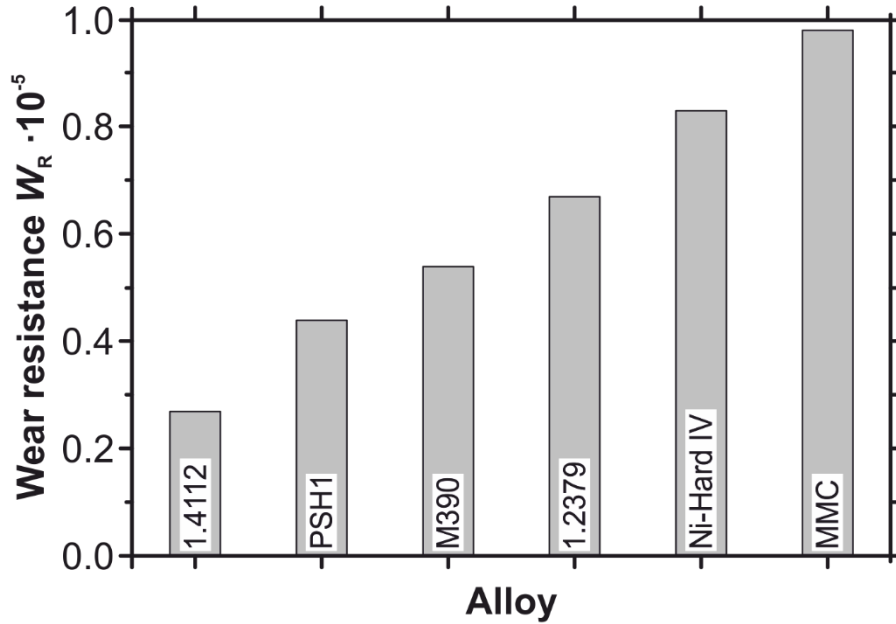


Figure 10. Comparison of the wear resistance W_R of PSH1 and MMC with 1.4112 (X90CrMoV18, AISI 440B), Böhler M390 (X190CrVMo20-4-1), 1.2379 (X155CrVMo12-1, AISI D2) and Ni-Hard IV (G-X300CrNiSi9-5-2, EN-JN2049). Whereas W_R of PSH1 is slightly below the level of the comparable corrosion-resistant cold-work tool steel M390, the MMC is superior to all other tested alloys, including the white cast iron Ni-Hard IV. All alloys were quenched and tempered at the SHM to obtain their maximum wear resistance.

Corrosion Resistance. Figure 11 shows representative potentiodynamic polarisation curves of the tested alloys (PSH1: solid line, MMC: dashed line) in comparison with the Böhler M390 (grey dotted line). This steel was quenched from 1150 °C as is standard in the industry. Figure 11(a) shows that the passive current density, ie the lowest current density in the plateau region, is below 10 $\mu\text{A}/\text{cm}^2$ and thus much lower than that of M390 (about 50 $\mu\text{A}/\text{cm}^2$). This indicates a high resistance to uniform surface corrosion. The passivation potential, represented by the first peak, and the OCP are almost the same for all three steels. The second peak in the curve of the M390 at about 200 mV/SHE is suggested to be the potential at which the matrix close to chromium-rich carbides is corroded because its chromium content is lower than that of the surrounding matrix [10,11]. This peak is missing for PSH1 and MMC because they do not contain any chromium-rich carbides. The small peak at about 600–700 mV/SHE is ascribed to corrosion of the mono-carbides, ie VC in M390 and NbC in PSH1 and MMC [12,42–45]. This peak appears for all three steels because they all contain such carbides. The transpassive region, represented by the sudden increase in current density at high potentials [12], of PSH1 and MMC starts at a considerably higher potential than that of M390 [41,42]. In combination with the missing second peak, this leads to a broad passive region between the passivation potential and the transpassive region. This is said to be favourable for a high corrosion resistance [42,46]. Thus the positive effect of NbC on the corrosion resistance of the newly developed steels is obvious from the measured curves.

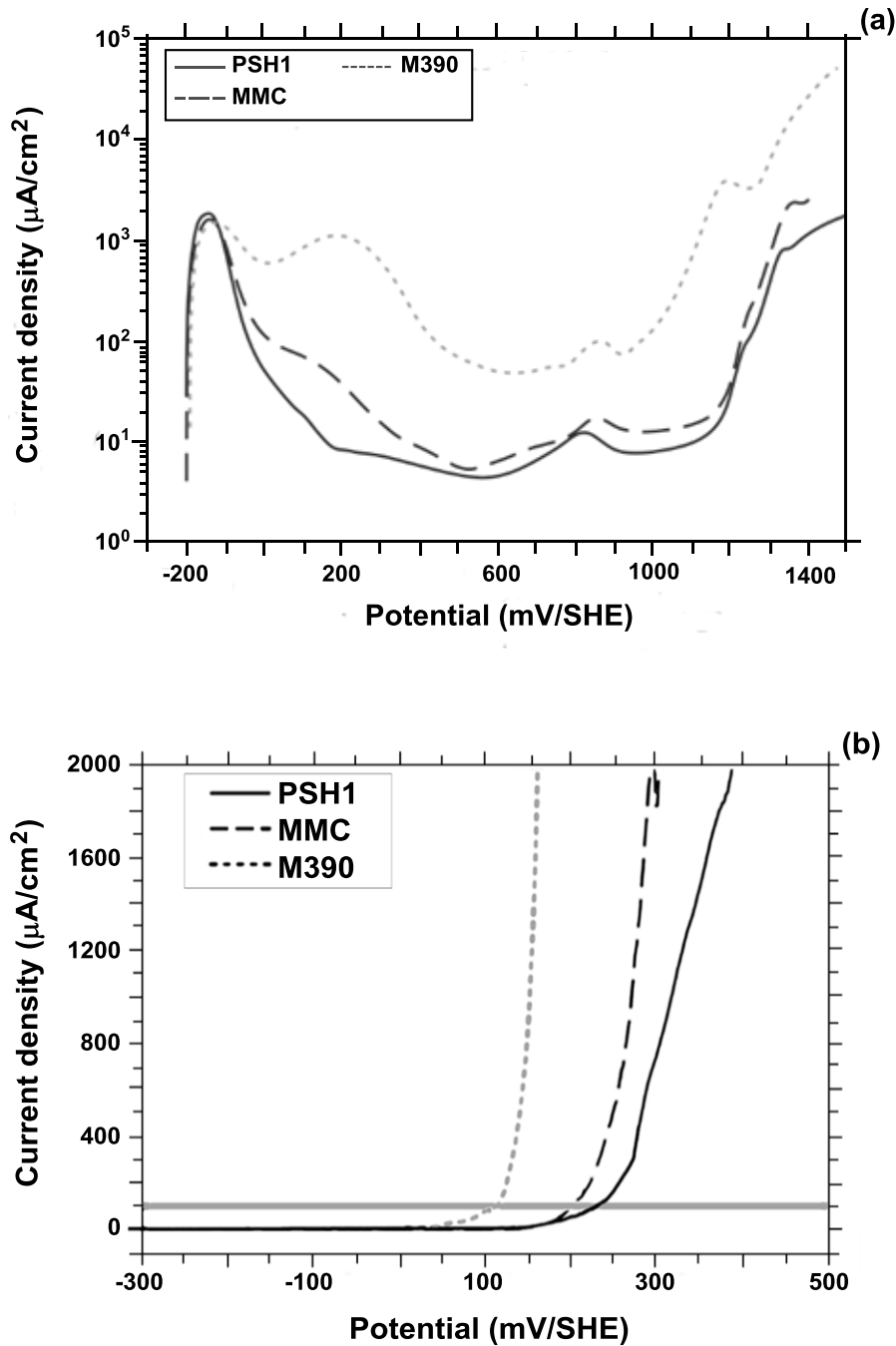


Figure 11. Representative potentiodynamic polarisation curves for PSH1 (solid line) and MMC (dashed line) in comparison with Böhler M390 (grey dotted line); (a) in H_2SO_4 and (b) in NaCl . PSH1 and MMC were quenched from $1100\text{ }^\circ\text{C}$, whereas T_{Aus} was $50\text{ }^\circ\text{C}$ higher for the M390 as in the standard in the industry. Figure 11(a) shows that the current density of the plateau region is considerably lower for PSH1 and MMC than for M390. Additionally, the plateau is broader. Both aspects indicate a better corrosion resistance for the newly developed steels. Figure 11(b) shows that PSH1 has the highest resistance against pitting corrosion followed by MMC and M390.

The corrosion behaviour in sulphuric acid is of interest for applications in the polymer industry. However, these steels could also be used in sea water environments as shown in the potentiodynamic polarisation curves measured in NaCl in Figure 11(b). The horizontal line at $100 \mu\text{A}/\text{cm}^2$ represents the threshold value defined above. Obviously, the common steel M390 shows the lowest corrosion resistance because the steep increase in current density, which indicates the onset of pitting corrosion, is located at the least noble potential (about 105 mV). It is followed by MMC (≈ 200 mV) and PSH1 (≈ 230 mV), where the latter shows a slightly nobler potential than the former. However, the steep increase of the curves starts at much lower potentials than in H_2SO_4 . This can be attributed to the pitting corrosion mechanism, which is much more sensitive to chromium depletion and inhomogeneities than uniform surface corrosion [24,47,48].

This behaviour is generally consistent with theory. The M390 is more prone to pitting corrosion owing to its lower molybdenum content, which is regarded as being especially effective in preventing pitting [15,17,49]. Additionally, the chromium-rich carbides lead to zones depleted of chromium, which act as starting points for pitting corrosion [10,11]. The difference between the pitting behaviour of PSH1 and MMC is small, but worthy of note. Since the matrix composition of both steels is the same, this difference has to be attributed to the admixed NbC. These are about one order of magnitude larger than the precipitated ones. As mentioned above, pitting corrosion in general is sensitive to inhomogeneities. This increases with increasing size of the inhomogeneities [50]. Thus, the MMC is more prone to pitting than PSH1.

Martensitic Stainless PM Bearing Steels for Extreme Loading and Lubrication Conditions

Development

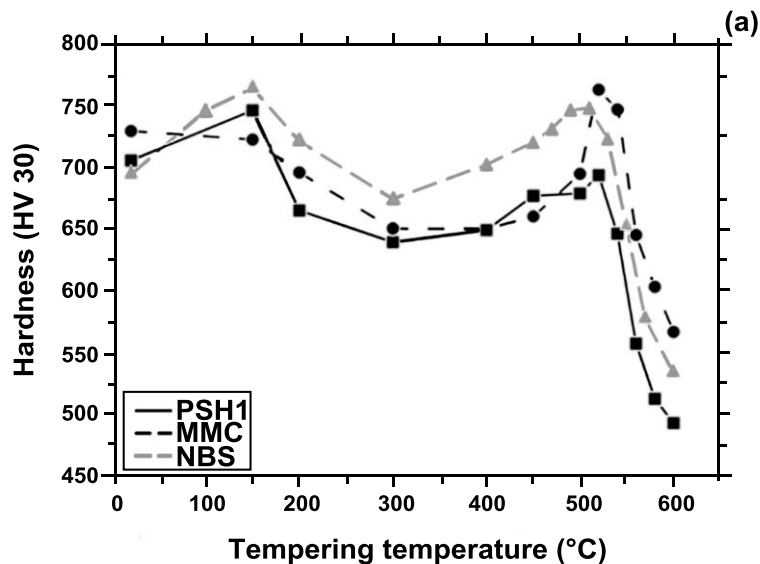
The new steels discussed above contain at least 10 vol.% carbides. This is not favourable for most bearing steels. One of the standard bearing steels is 1.3505 (100Cr6, AISI 52100), which contains about 2–3 vol.% after an adequate heat treatment. These are beneficial for the wear resistance in bearing lifetime tests [51]. Thus, the aim is to develop new steels with a carbide content of below 5 vol.%. However, as mentioned above, manufacturing by means of diffusion alloying allows almost arbitrary adjustment of the carbide content of PSH1 to the required value. Thus, a steel of similar composition to PSH1, but with a considerably lower amount of niobium would be an appropriate bearing steel. For a higher resistance to sea water, which can be simulated with NaCl [33], Equation 2 indicates that more chromium and molybdenum should be useful. However, because both elements stabilise ferrite, additional elements are required for the stabilisation of austenite. The newly developed steel is designated below as NBS (new bearing steel). The hardness of bearing steels has to be higher than 650 HV. The fine dispersion of carbides together with the generally fine microstructure of a PM steel should be beneficial for this application, not least for the necessary hot working processes in manufacturing. The final composition of the investigated steel is not given here for reasons of confidentiality.

Experimental

The experimental work was performed in accordance with the work described above, but in addition, the steel was forged after HIP. However, the heat treatment had to be adjusted to the new steel resulting in a slightly higher T_{Aus} , as well as slightly different tempering temperatures. The hardness was measured for several T_{Aus} and carbon contents. This led to the final adjustment of the desired carbon content and thus the amount of carbides, which is again not given here. A high resistance to abrasive wear is beyond the scope of most bearing steels. Thus, no wear tests were performed. However, tribocorrosion tests might be of interest for the NBS. Of course, the alloying concept could be favourable for wear-resistant bearing steels, eg for highly grease-lubricated bearings in heavily contaminated environments, such as those that apply for bucket-wheel excavators.

Results and Discussion

Hardness and Microstructure. Figure 12(a) shows a tempering curve of the NBS (grey dashed line) after quenching from an adequate T_{Aus} in comparison to PSH1 (solid line) and MMC (black dashed line). The hardness is in the range of that of PSH1 and MMC and even slightly above it. Thus, the hardness of the NBS considerably exceeds the required value of 650 HV. Good corrosion resistance should be obtained for tempering at low temperatures, ie up to 200 °C [52], whereas tempering at the SHM (at 520 °C) should increase the wear resistance. Figure 12(b) shows the microstructure of the NBS. The only carbides are NbC and their amount is obviously reduced compared to PSH1 and MMC (Figure 7). Some carbides seem to be accumulated and elongated in the vertical direction. This is due to the forging process, which elongates the carbides in the forging direction. In addition, the NbC is finely dispersed in the martensitic matrix. The black spots in the matrix are oxides and not pores.



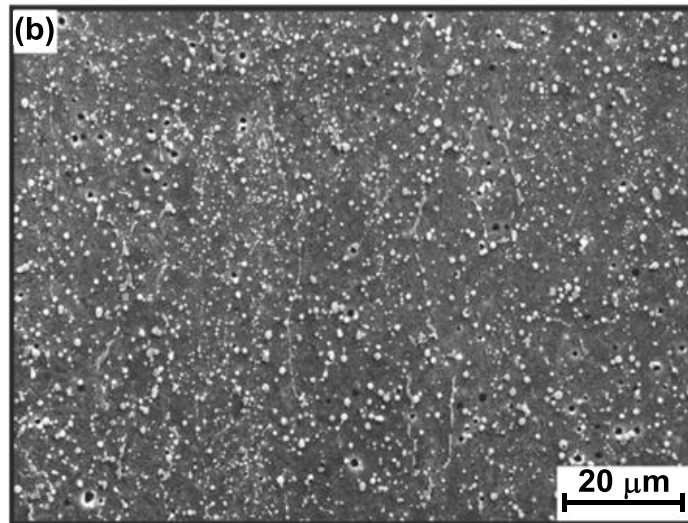


Figure 12. (a) Tempering curve of NBS (grey dashed line). Its hardness is in the range of that of PSH1 (solid line) and MMC (black dashed line) and well above 650 HV. (b) Microstructure of the new bearing steel. As intended, the content of NbC is reduced in comparison to PSH1 and MMC.

Corrosion Resistance. Figure 13 shows representative potentiodynamic polarisation curves of the NBS (grey dashed line) in comparison to those curves already shown in Figure 11. Obviously, its corrosion resistance is higher than that of the common steel M390, but lower than that of PSH1 and MMC. The curve shows a peak at about 200 mV/SHE indicating chromium-rich carbides in the matrix. It might also be attributable to chromium depletion around the oxides found in the matrix, Figure 12(b). Whereas those shown above are fairly small, considerably larger oxides (20–30 μm) were also found to some extent. These need to be addressed upon moving from the current model alloy to industrially applicable material. These could also be detrimental for the general corrosion resistance, ie the higher passive current density of the plateau region [53]. The passivation peak of the NbC at about 600–700 mV/SHE is missing or is only indistinct. This might be due to the lower amount of NbC than in PSH1 and MMC, in combination with the higher passive current density. However, the plateau is still broader than that of the M390, indicating a better corrosion resistance [42,46]. Furthermore, the corrosion resistance of the NBS is higher than that of the other tested alloys (≈ 260 mV). This can be attributed to the higher amount of chromium and molybdenum in this steel, in comparison to PSH1 and MMC [15,17,49]. However, the difference is comparatively small with respect to the differences in the contents of chromium (2 wt.%) and molybdenum (1 wt.%). This might be attributable to the existence of oxides in the NBS, which additionally lower the resistance to pitting corrosion [53]. Thus, the amount of oxides in the NBS has to be lowered to further improve its corrosion resistance. This would also be beneficial for the bearing lifetime with regard to improved wear resistance.

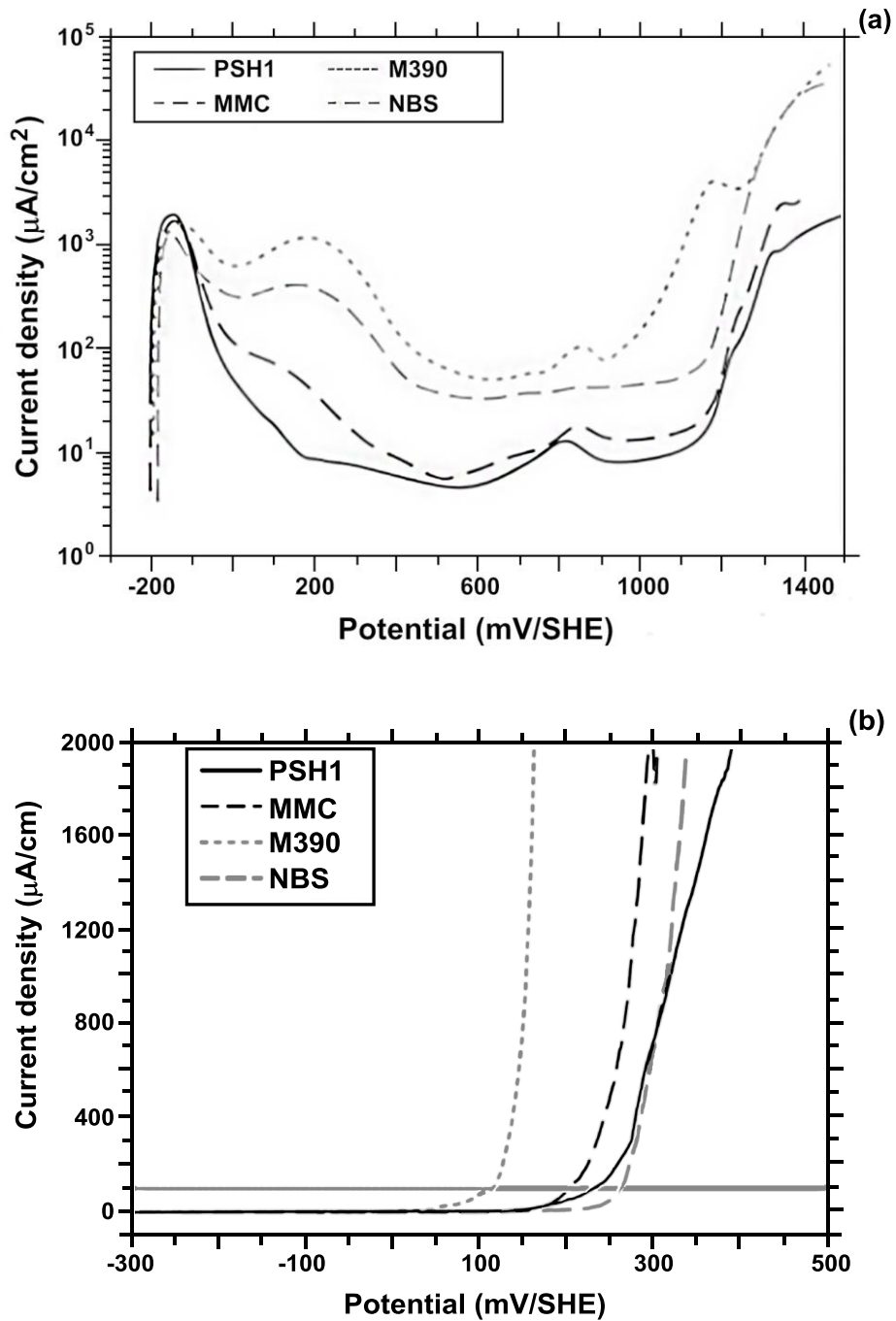


Figure 13. Representative potentiodynamic polarisation curves for NBS (grey dashed line) compared to the curves shown in Figure 11; (a) in H₂SO₄ and (b) in NaCl. The NBS was tested in the as-quenched condition that is comparable to the other three steels. In H₂SO₄, the corrosion resistance of the NBS is higher than that of M390, but lower than that of PSH1 and MMC. In NaCl the NBS shows the highest corrosion resistance of all four alloys.

Conclusions

The present study deals with the development of corrosion-resistant tool steels for the polymer and bearing industries. Diffusion alloying is introduced as a new way of manufacturing niobium-rich steels. The main conclusions are:

1. Diffusion alloying can be used to produce niobium-rich steels without huge primary NbC in the microstructure. In fact, a fine dispersion of NbC with a size of about 1-3 μm will result after HIP.
2. With diffusion alloying, the content of hard phases can be almost arbitrarily adjusted by admixing different amounts of carbon. Thus, steels with a high corrosion resistance, as well as a high wear resistance can be produced from the same steel powder. Furthermore, a metal matrix composite can easily be produced by admixing additional hard phases such as NbC.
3. The highest corrosion resistance is expected for quenching from the γ +MC phase field because the NbC contains only small amounts of chromium and molybdenum, which thus remain dissolved in the matrix.
4. All investigated steels show a high hardness and wear resistance. The resistance of the MMC against coarse abrasives is even higher than that of the white cast iron Ni-Hard IV.
5. The resistance of all investigated steels against uniform surface corrosion and pitting corrosion is considerably higher than that of a comparable common steel.
6. The development of a corrosion-resistant powder-metallurgical bearing steel containing NbC was possible by adjusting the alloying system. The hardness and corrosion resistance of this steel seem to be promising for possible applications in sea water environments, although further development is necessary.

Acknowledgements

Parts of this contribution were financed by the industrial partner Böhler Edelstahl GmbH & Co KG. Others were part of a joint research project (reference no. 03ET1072D) funded by the Federal Ministry for Economic Affairs and Energy. The authors gratefully acknowledge financial support by the BMWi.

References

1. H. Berns and W. Theisen, *Ferrous Materials – Steel and Cast Iron* (Springer Verlag, 2008).
2. W. Theisen, S. Siebert and S. Huth, “Wear Resistant Steels and Casting Alloys Containing Niobium Carbide,” *Steel Research International*, 78 (12) (2007), 921-928.
3. W. Theisen, *Bearbeiten verschleißbeständiger Legierungen aus werkstofftechnischer Sicht* (VDI, Düsseldorf, 1997).

4. H. Berns, ed, *Hartlegierungen und Hartverbundwerkstoffe: Gefüge, Eigenschaften, Bearbeitung, Anwendungen* (Springer Berlin Heidelberg, 1998).
5. G.C. Coelho, J.A. Golczewski and H.F. Fischmeister, "Thermodynamic Calculations for Nb-containing High-speed Steels and White-cast-iron Alloys," *Metallurgical and Materials Transactions A*, 34A (2003), 1749-1758.
6. F. Heisterkamp and S.R. Keown, "Niobium in High-speed Tool Steels," *Processing and Properties of High Speed Tool Steels: Proceedings of a Symposium by the Ferrous Metallurgy Committee of The Metallurgical Society of AIME at the 109th AIME Annual Meeting*, ed M.G.H. Wells and L.W. Lherbier (Las Vegas, NV: The Metallurgical Society of AIME, 1980), 104-123.
7. S. Karagöz and H.F. Fischmeister, "Niobium-alloyed High-speed Steel by Powder-metallurgy," *Metallurgical Transactions A*, 19 (6) (1988), 1395-1401.
8. C. Kerschenbauer et al., "PM Plastic Mould Steels," *The Use of Tool Steels: Experience and Research: Proceedings of the 6th International Tooling Conference*, ed J. Bergström et al., (Karlstad University, Motala Grafiska AB, Motala, 2002), 293-301.
9. DIN EN 10088: "Nichtrostende Stähle," Beuth Verlag, 2005.
10. H. Schüller, P. Schwaab and W. Schwenk, "Die Potentialabhängigkeit der interkristallinen Korrosion eines angelassenen austenitischen Chrom-Nickel-Stahls," *Archiv für das Hüttenwesen*, 33 (12) (1962), 853-862.
11. A. Bäuml et al., "Deutung der Ursachen der interkristallinen Korrosion von nichtrostenden Stählen in Zusammenhang mit der Chromverarmungstheorie," *Corrosion Science*, 4 (4) (1964), 89-103.
12. G. Herbsleb, "Der Einfluß von Legierungselementen auf das Passivierungsverhalten nichtrostender Stähle," *VDI-Zeitschrift*, 123 (12) (1981), 505-511.
13. S. Huth, N. Krasokha and W. Theisen, "Development of Wear and Corrosion Resistant Cold-work Tool Steels Produced by Diffusion Alloying," *Wear*, 267 (2009), 449-457.
14. R.F.A. Jargelius-Petterson and B.G. Pound, "Examination of the Role of Molybdenum in Passivation of Stainless Steels Using AC Impedance Spectroscopy," *Journal of the Electrochemical Society*, 145 (5) (1998), 1462-1469.
15. J.N. Wanklyn, "The Role of Molybdenum in the Crevice Corrosion of Stainless Steels," *Corrosion Science*, 21 (3) (1981), 211-225.
16. M. Urquidi and D.D. Macdonald, "Solute-vacancy Interaction Model and the Effect of Minor Alloying Elements on the Initiation of Pitting Corrosion," *Journal of the Electrochemical Society*, 132 (3) (1985), 555-558.

17. R.C. Newman, "The Dissolution and Passivation Kinetics of Stainless Alloys Containing Molybdenum - II. Dissolution Kinetics in Artificial Pits," *Corrosion Science*, 25 (5) (1985), 341-350.
18. S. Huth, "Entwicklung neuer pulvermetallurgischer Stähle für Anwendungen unter Verschleiß- und Korrosionsbeanspruchung" (Ph.D. thesis, Ruhr-Universität Bochum, 2009).
19. W. Theisen et al, "Verschleißbeständiger Werkstoff," Austrian Patent No. AT 507 215 B1 2010-03-15, (2009), held by Böhler Edelstahl GmbH & Co KG.
20. K.W. Andrews, "Empirical Formulae for the Calculation of Some Transformation Temperatures," *Journal of the Iron and Steel Institute*, 203 (7) (1965), 721-727.
21. C.Y. Kung and J.J. Rayment, "An Examination of the Validity of Existing Empirical Formulae for the Calculation of Ms Temperature," *Metallurgical and Materials Transactions A*, 13A (1982), 328-331.
22. N. Krasokha and H. Berns, "Study on Nitrogen in Martensitic Stainless Steels: Studie über Stickstoff in Martensitischen Rostfreien Stählen," *HTM*, 66 (3) (2011), 150-164.
23. V. Raghavan, "C-Fe-Nb (Carbon-Iron-Niobium)," *Journal of Phase Equilibria*, 24 (1) (2003), 57-61.
24. J.N. Bernauer, "Einfluss von Kohlenstoff als Legierungselement in stickstofflegierten Chrom-Mangan-Stählen" (Ph.D. thesis, ETH Zürich, 2004).
25. J.N. Bernauer (2004) Einfluss von Kohlenstoff als Legierungselement in stickstofflegierten Chrom-Mangan-Stählen, Zürich.
26. S. Huth and W. Theisen, "High Nitrogen PM Tool Steels Containing Niobium," *Proceedings of 10th International Conference on High Nitrogen Steels*, ed A.G. Svyazhin, V.G. Prokoshkina and K.L. Kosyrev (MISIS, Moscow, 2009), 90-95.
27. V.G. Gavriljuk and H. Berns, *High Nitrogen Steels: Structure, Properties, Manufacture, Applications* (Springer Berlin, 1999).
28. F. Jeglitsch, "Niobium in Tool Steels and Cemented Carbides," *Niobium Science and Technology: Proceedings of the International Symposium Niobium 2001*, ed Niobium 2001 Limited (Orlando, FL, 2001), 1001-1039.
29. T. Schneiders, "Neue pulvermetallurgische Werkzeugstähle" (Ph.D. thesis, Ruhr-Universität Bochum, 2005).
30. H. Berns, "Verfahren zur Herstellung von PM-Hartlegierungen (Process for the Production of PM Hard Alloys)," German Patent No. DE 42 35 148 C1 (1992).

31. S. Huth, "Entwicklung neuer pulvermetallurgischer Stähle für Anwendungen unter Verschleiß- und Korrosionsbeanspruchung" (oral presentation of Ph.D. thesis, Ruhr-Universität Bochum, 2009).
32. S. Huth et al., "Oxide Reduction during Carburization Nb-rich Tool Steel Powders for Diffusion Alloying," *Euro PM: Congress & Exhibition*, ed European Powder Metallurgy Association (Shrewsbury, 2012), 507-512.
33. DIN 50905-1: "Korrosionsuntersuchungen - Grundsätze," Beuth Verlag, 1987.
34. ASTM International G 150-99: "Standard Test Method for Electrochemical Critical Pitting Temperature Testing of Stainless Steel," ASTM, 2006.
35. M. Vayer, I. Reynaud and R. Erre, "XPS Characterisations of Passive Films Formed on Martensitic Stainless Steel: Qualitative and Quantitative Investigations," *Journal of Materials Science*, 35 (35) (2000), 2581-2587.
36. D. Peckner and I.M. Bernstein, *Handbook of Stainless Steels* (McGraw-Hill, New York, 1977).
37. H. Berns, G. Siekmann and I. Wiesenecker, "Gefüge und Bruch vergüteter Federstähle: Gefüge und Bruchmorphologie," *Draht*, 35 (5) (1984), 247-252.
38. H.K.D.H. Bhadeshia and R.W.K. Honeycombe, *Steels: Microstructure and Properties*, (Elsevier/Butterworth-Heinemann, Amsterdam, 2006).
39. H.F. Fischmeister, S. Karagöz and H. Andrén, "An Atom Probe Study of Secondary Hardening in High Speed Steels," *Acta Metallurgica*, 36 (4) (1988), 817-825.
40. N. Axén and K. Zum Gahr, "Wear of TaC and TiC Steel Composite Hardfacings by Soft and Hard Abrasives," *Materialwissenschaft und Werkstofftechnik*, 23 (10) (1992), 360-367.
41. S. Huth et al., "Novel Corrosion- and Wear-resistant PM Plastic Mould Steels Containing NbC," *Proceedings of the 8th International Tooling Conference: Tool Steels - Deciding Factor in Worldwide Production*, ed P. Beiss et al. (Aachen, Verlag Mainz, Wissenschaftsverlag, 2009), 425-435.
42. S. Huth, H. Hill and W. Theisen, "Corrosion of Stainless PM Tool Steels: Interpretation of Current Density Potential Curves in Acid Environments," *HTM*, 65 (4) (2010), 195-200.
43. S. Süry and T. Geiger, "Einfluß der Wärmebehandlung auf den Verlauf der Stromdichte-Potential-Kurven bei einem 13%-igen Chromstahlguss," *Werkstoffe und Korrosion*, 20 (8) (1969), 665-672.
44. A. Sehgal, B.G. Ateya and H.W. Pickering, "Hydrogen Evolution and Absorption within Grain Boundary Grooves in Sensitized Stainless Steel under Condition of Anodic Polarization," *Journal of the Electrochemical Society*, 142 (10) (1995), L198-L200.

45. W.K. Kelly, R.N. Iyer and H.W. Pickering, "Another Grain Boundary Corrosion Process in Sensitized Stainless Steel," *Journal of the Electrochemical Society*, 140 (11) (1993), 3134-3140.
46. H. Kaesche, *Corrosion of Metals: Physicochemical Principles and Current Problems* (Springer Verlag, 2003).
47. H.J. Cleary and N.D. Greene, "Corrosion Properties of Iron and Steel," *Corrosion Science*, 7 (7) (1967), 821-831.
48. Y. Tan, "Understanding the Effects of Electrode Inhomogeneity and Electrochemical Heterogeneity on Pitting Corrosion Initiation on Bare Electrode Surfaces," *Corrosion Science*, 53 (5) (2011), 1845-1864.
49. P. Schmuki, "From Bacon to Barriers: A Review on the Passivity of Metals and Alloys," *Journal of Solid State Electrochemistry*, 6 (2002), 145-164.
50. G.T. Burstein and G.O. Ilevbare, "The Effect of Specimen Size on the Measured Pitting Potential of Stainless Steel," *Corrosion Science*, 38 (12) (1996), 2257-2265.
51. H.K.D.H. Bhadeshia, "Steels for Bearings," *Progress in Materials Science*, 57 (2) (2012), 268-435.
52. M. Seifert et al., "Corrosion Properties of a Complex Multi-phase Martensitic Stainless Steel Depending on the Tempering Temperature," accepted for publication in: *Materials and Corrosion*, DOI:10.1002/maco.201508229.
53. E. Klar and P. Samal, *Powder Metallurgy Stainless Steels: Processing, Microstructures, and Properties* (Materials Park, OH: ASM International, 2007).